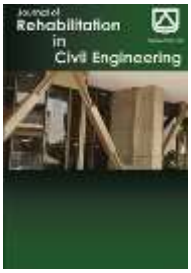

journal homepage: http://civiljournal.semnan.ac.ir/

Investigating of the Effect of Concrete Confinement on the Axial Performance of Circular Concrete Filled Double-Skin Steel Tubular (CFDST) Long Columns

H. Saberi[1*], V. Kolmi Zadeh[2], A. Mokhtari[3] and V. Saberi[4]

1. Assistant Professor, Faculty of Civil Engineering, University of Eyvanekey, Semnan, Iran
2. Masters, Structural Engineer, Faculty of Civil Engineering, University of Eyvanekey, Semnan, Iran
3. Masters, Structural Engineer, Faculty of Civil Engineering, University of Eyvanekey, Semnan, Iran
4. Assistant Professor, Faculty of Civil Engineering, University of Eyvanekey, Semnan, Iran

Corresponding author: saberi.hamid@gmail.com

ARTICLE INFO

Article history:
Received: 25 November 2019
Accepted: 06 February 2020

Keywords:
Composite Columns,
CFDST Columns,
Axial Performance,
Circular Columns,
Confinement Effect.

ABSTRACT

In this study, the co-operation of steel and concrete in composite columns is considered. Using numerical modeling to study the behavior of these sections, a new type of sections, namely Concrete Filled Double-Skin steel Tubular (CFDST) columns, is introduced. The parameters and techniques that influence the numerical simulation that bring this modeling closer to the laboratory conditions are determined by varying the dimensions and geometry as well as the properties of materials such as the compressive strength of concrete and width to thickness ratio on the strength of circular section columns at internal and external skins are investigated by the ABAQUS finite element software. The purpose of this paper is to investigate the effect of concrete compressive strength on the axial performance of CFDST columns. In this paper, the effects of concrete with different compressive strength, concrete confinement, bearing capacity and width-to-thickness ratio on the overall strength of tubular cross-section columns in their inner and outer skins are investigated. The results of the study indicated that the bearing capacity of CFDST columns under axial pressure increases by increasing the concrete compressive strength in the inner skin and decreases by increasing width to thickness ratio (D/t). Also, studies have shown that with increasing cross-sectional area, the bearing capacity in circular columns decreases by about 3%.

1. Introduction

In recent years, a concept called Concrete filled double-skin steel tubular CFDST columns has been developed. This idea was taken from steel-concrete-steel sandwich (SCSS) and Concrete filled tubes (CFT) [1].

DOI: 10.22075/JRCE.2020.19167.1362

CFDSTs have recently been considered for use in docks and high bridge piers in deep valleys of Japan to reduce the weight of structures, while retaining much energy absorption capacity against seismic loading. It is also possible to use CFDST in columns of structures as a composite bridge pillar in marine applications. Compared to the enclosure of reinforced concrete columns, CFDST columns impose a more robust and uniform compression on internally filled concrete by steel walls, which reduces the problem of steel density and improves concrete quality [2]. As with the sandwich structure (placement of a substance between the two other materials), another advantage of CFDST is that the loop formed between steel pipes means that a variety of filler materials can be used for various applications [3]. Therefore, numerical and laboratory studies on the behavior of CFDST columns have recently been carried out by researchers, such as the empirical study on concrete-less internal walls with SHS-SHS and CHS-CHS cross sections, performed by Zhao and Grzebieta [4] and Elchalakani et al. [5]. But the first laboratory study on CFDST columns with the CHS-CHS section was developed by Tao et al. in 2004 [6], in which the compressive strength of concrete was 40MPa, and for each sample, the steel tubulars had the same thickness. Han et al. In 2011 [7] studied CFDST columns under long-term stable loading conditions, with the results that long-term loading reduces the ultimate strength of CFDST columns while increasing the ductility. Dundu et al. in 2015 [8] conducted studies on CFDST long column under axial loads with normal strength concrete; Also, Romero et al. In 2015 [9] studied on CFDST column with high strength concrete. Romero et al. in 2017 [10] looked at circular columns with extremely high resistance under off-center loads. Wan and Zha in 2017 [11] examined the results of empirical data in double-skin steel columns under axial loads. Ghanim Hasan et al. In 2019 [12] experimentally investigated the effect of the inner wall on the behavior of CFDST columns, and the results were that CFDST columns could perform better than CFST columns when using the proper geometric shape of the inner steel pipe. Furthermore, the inner tube works consistently with the shell concrete and plays an important role in mitigating failure mode of CFDST even with high strength concrete (HSC). Also, Li et al. [13] and Vernardos et al. [14] and Yang et al. [15] have studied the behavior of CFDST columns in 2019. Considering that quantitative investigations have been carried out on CFDST columns, while their proper seismic performance increases their potential for high structures, due to their proper capacity and formability, this paper focuses on the behavior of these types of columns based on the materials used.

Since no studies have been conducted to investigate the increase in cross-sectional area and the impact of compressive strength of concrete on long CFDST columns, this study is distinguished from other studies. The purpose of this study was to investigate the behavior of circular CFDST columns under parameters such as compressive strength of concrete in the inner and outer tube, increase in cross-section area, as well as the thickness of the inner tube in these columns under axial force. It is worth noting that validation of the results obtained from the analysis of circular CFDST columns is performed using finite element software due to the lack of experiment; therefore, the validated model is in good agreement with the laboratory sample. Finally, the results showed that the

changes in tube thickness are far more important.

2. Verification Study

2.1. Verification Model

To solve the equations, the ABAQUS software [20] uses a variety of numerical methods. This parameter actually represents the numerical method used by the program to solve the equations for the desired element. Some numerical methods will inevitably bring about a large proportion of approximates for increasing the computational speed; hence, with proper accuracy and considering the computational cost, a proper method should be adopted. Nonlinear numerical simulations are performed based on finite element method using standard ABAQUS 2016 bundle. In this research, in order to ensure the accuracy of software modeling in finite element software, the results were compared with the experimental work by Romero et al., 2017 [16]. The dimensions and geometry of this laboratory sample are shown in Figure 1. After assuring the modeling accuracy, including loading, supporting conditions, materials and interaction of materials, designing and modeling of CFDST columns and studying the behavior of these columns under axial load with different compressive strength of the concrete, were carried out. In this regard, the results of the numerical analysis of the CFDST column and the laboratory sample mentioned in Table 1 are compared Figure 2 shows the displacement loading diagram for the mentioned sample along with experimental results.

Fig. 1. Details specimen experimental [16].

Table 1. Dimensions of the test specimens [16].

ID	Column specimen	Outer tube				Inner tube			
		D_{ext} (*mm*)	t_{ext} (*mm*)	$f_{y,ext}$ (*MPa*)	$f_{c,ext}$ (*MPa*)	D_{int} (*mm*)	t_{int} (*mm*)	$f_{y,int}$ (*MPa*)	$f_{c,int}$ (*MPa*)
NR2	C200-3-30-C114-8-30	200	3	332	45	114.3	8	403	42

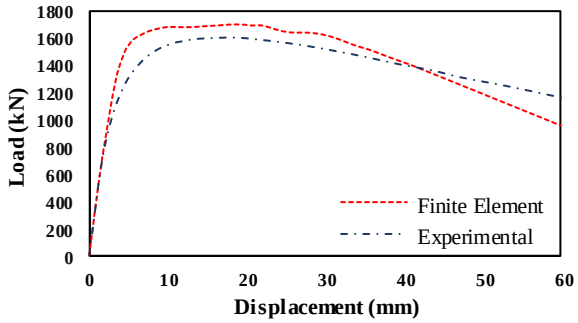

Fig. 2. experimental specimens load-axial curves and numerical model NR2.

Table 2. Comparisons between the experimental [16] and FE ultimate load.

	P_{EXP}	P_{FEM}
Sample NR2	1611	1708.02
Difference **(%)**	6.02%	

Table 2 shows the values of final load capacity obtained from laboratory and numerical results. Considering the difference of 6.02% between the finite element (P_{FEM})

and laboratory results, and final load capacity (P_{EXP}) for the NR2 sample, as well as the comparison of numerical and sample behavior shown in Fig. 2, the numerical model is well-matched. As a result, a proposed 3 dimensional element model can be used with acceptable precision to predict the behavior of CFDST.

2.2. Steel Modeling

ST-37 steel is used for modeling columns. For modeling of steel using the Ramberg-Osgood model, obtained by Elchalakani et al is used. [17]. The Ramberg-Osgood model involves the creation of an engineering stress-strain curve, after which the true strain curve shown in Fig. 3 is corrected. The coefficient (n) of the Ramberg-Osgood model is obtained by the following equation:

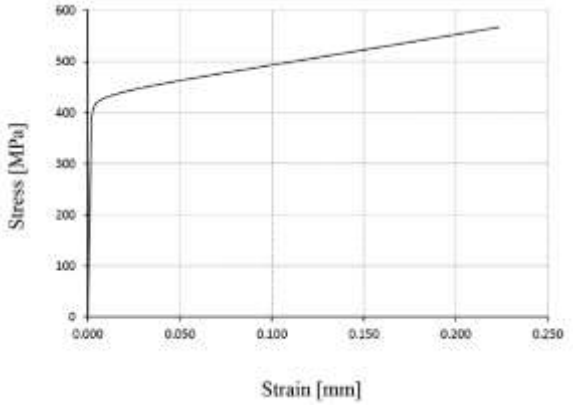

Fig. 3. Typical Ramberg-Osgood stress-strain curves [17].

$$\varepsilon = \frac{\sigma}{E} + 0.002\left(\frac{\sigma}{F_{ty}}\right)^{n} \quad (1)$$

In the finite element analysis, metallic materials are considered to be elastic materials until they reach yield stress. After that point, they are simulated as plastic materials. The elastic modulus (E) is equal to 203GPa, recommended by AISC 360-10 [18] and Poisson's ratio (ν) is 0.3.

2.3. Concrete Modeling

In ABAQUS software, three models of plastic behavior, crack expansion and fading crack are used for concrete modeling. In this research, Damage Plasticity Behavior Model (CDP) is used for modeling concrete. This model is based on the hardening and softening behavior of semi-brittle materials such as concrete [19]. Due to the interaction between concrete and steel in columns filled with concrete, a three-axis stress state is created in the concrete core, which is dependent on the concrete enclosure [21,22]. To illustrate the interaction effects between steel and concrete in Fig. 4, the CFDST column is presented [23].

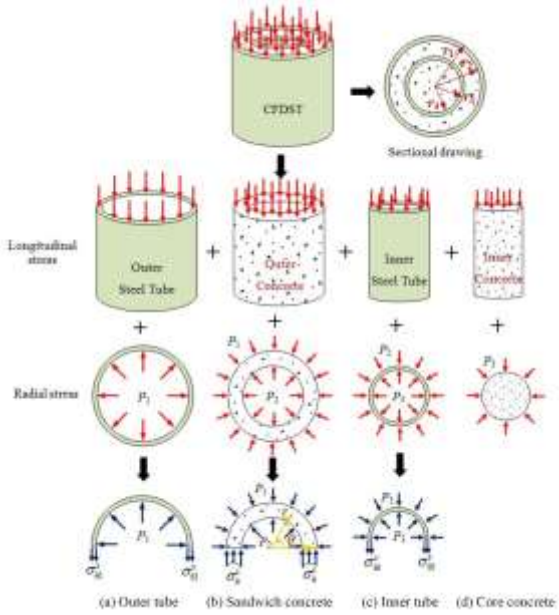

Fig. 4. The stress analysis diagram [23].

2.3.1. External Concrete

The enclosed concrete was used for the external concrete modeling process of the samples. The concrete used is of model presented by Pagoulatou et al. [24], which was later introduced as the Pagoulatou model. The concrete model proposed by

Pagoulatou et al. [24,25], as shown in Fig. 5, contains a series of the following equations:

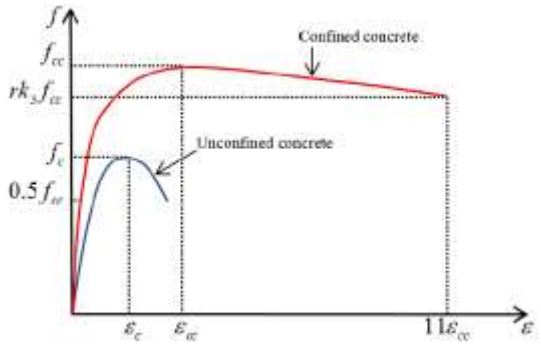

Fig. 5. Stress-strain curves for concrete Pagoulatou, et al. [24,25].

$$f_{cc} = f_c + k_1 f_1 \tag{2}$$

$$\varepsilon_{cc} = \varepsilon_c (1 + k_2 \frac{f_1}{f_c}) \tag{3}$$

$$f_1 = 8.525 + 0.166(\frac{B_0}{t_0}) - 0.00897(\frac{B_i}{t_i}) + 0.00125(\frac{B_0}{t_0})^2 + 0.00246(\frac{B_0}{t_0})(\frac{B_i}{t_i}) - 0.0055(\frac{B_i}{t_i})^2 \geq 0 \tag{4}$$

$$\frac{f_1}{f_{yi}} = 0.01844 - 0.00055(\frac{B_0}{t_0}) - 0.0004(\frac{B_i}{t_i}) + 0.00001(\frac{B_0}{t_0})^2 + 0.00001(\frac{B_0}{t_0})(\frac{B_i}{t_i}) - 0.00002(\frac{B_i}{t_i})^2 \tag{5}$$

$$\frac{f_1}{f_{yo}} = 0.01791 - 0.00036\left(\frac{B_0}{t_0}\right) - 0.00013(\frac{B_i}{t_i}) + 0.00001(\frac{B_0}{t_0})^2 + 0.00001(\frac{B_0}{t_0})(\frac{B_i}{t_i}) - 0.00002(\frac{B_i}{t_i})^2 \tag{6}$$

$$\sigma_{Concrete} = \frac{E_c \varepsilon}{1 + (R + R_e - 2)\left(\frac{\varepsilon}{\varepsilon_{cc}}\right) - (2R - 1)\left(\frac{\varepsilon}{\varepsilon_{cc}}\right)^2 + R\left(\frac{\varepsilon}{\varepsilon_{cc}}\right)^3} \tag{7}$$

$$E_c = 4700\sqrt{f_{cc}} \tag{8}$$

$$R = \frac{R_E(R_\sigma - 1)}{(R_\varepsilon - 1)^2} - \frac{1}{R_\varepsilon} \tag{9}$$

$$R_E = \frac{E_c \varepsilon_{cc}}{f_{cc}} \tag{10}$$

2.3.2. Internal Concrete for Circular Sections

The strain curve shown in Fig. 6 [26] was used in finite element analysis, which is proposed by Liang and Fragomeni [27]:

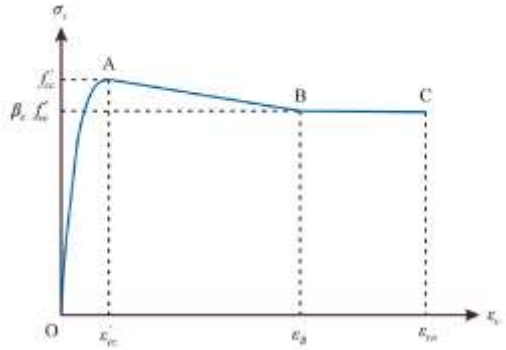

Fig. 6. concrete Stress-strain curves for circular cross-section [22].

In this model, the driving effect of concrete increases the strength and flexibility of concrete. The OA section of the strain stress curve is presented using the equations proposed by Mander and colleagues [28]. We have:

$$\sigma_c = \frac{f'_{cc}\lambda(\varepsilon_c/\varepsilon'_{cc})}{\lambda - 1/0 + (\varepsilon_c/\varepsilon'_{cc})^\lambda} \tag{11}$$

$$\lambda = \frac{E_c}{E_c - (f'_{cc}/\varepsilon'_{cc})} \tag{12}$$

In the above, is longitudinal compression of concrete, f'_{cc} is compressive strength in enclosed concrete, ε_c is longitudinal compressive strain of concrete, ε_{cc} is strain in f'_{cc} and E_c is modulus of Young, determined by the recommendations in ACI 318 [29], which are defined by the equation (13):

$$E_c = 3320\sqrt{\gamma_c f'_c} + 6900 \tag{13}$$

In which γ_c is a reducing strength factor for column size effects, concrete quality and loading rate in concrete compressive strength. This factor (γ_c) is given by Liang [30] on the basis of the following equation:

$$\gamma_c = 1/85 D_c^{-0/135} \quad (0/85 \le \gamma_c \le 1/0) \tag{14}$$

In the above formula, Dc is the diameter of the concrete core.

The strength of enclosed concrete (f'_{cc}) and the related strain (ε'_{cc}) have been proposed by Mander et al. [28]. Using the strength reduction coefficient, the equation is as follows [30]:

$$f'_{cc} = \gamma_c f'_c + k f'_{rp} f'_{cc} \tag{15}$$

$$\varepsilon'_{cc} = \varepsilon'_c \left[1 + 5k \frac{f'_{rp}}{\gamma_c f'_c} \right] \tag{16}$$

The value of *k* was determined by Richart et al. [31] to be 4.1. ε_{cc} represents strain in the non-enclosed concrete f'_{cc} and can be defined as follows:

$$\varepsilon'_c = \begin{cases} 0/002 & \gamma_c f'_c \le 28(MPa) \\ 0/002 + \dfrac{\gamma_c f'_{cc} - 28}{54000} & 28 < \gamma_c f'_c \le 82(MPa) \\ 0/003 & \gamma_c f'_c > 82(MPa) \end{cases} \tag{17}$$

An enclosed pressure model for conventional and high-strength concrete by a conventional or high-strength steel tube is proposed by Liang and Fragomeni [27], according to Hu et al. [32] and Tang et al. [33]. This numerical equation is as follows:

$$f'_{rp} = \begin{cases} 0/7(v_e - v_s)\dfrac{2t}{D-2t} f_{sy} & \dfrac{D}{t} \le 47 \\ \left(0/006241 - 0/0000357 \dfrac{D}{t}\right) f_{sy} & 47 < \dfrac{D}{t} \le 150 \end{cases} \tag{18}$$

In the above equation D is the outer diameter of the steel tube, t is the wall thickness of the steel tube, v_e and v_s are Poisson ratios of a steel wall with concrete and no concrete filler. The Poisson's ratio v_s is taken as 0.5 at the maximum strength point and v_e is given by Tang et al. [33]. The AB and BC sections of Figure 6 show the stress-strain curve, which is as follows:

$$\sigma_c = \begin{cases} \beta_c f'_{cc} + \left(\dfrac{\varepsilon_B - \varepsilon_c}{\varepsilon_B - \varepsilon'_{cc}} \right) (f'_{cc} - \beta_c f'_{cc}) & \varepsilon'_{cc} < \varepsilon_c \le \varepsilon_B \\ \beta_c f'_{cc} & \varepsilon_c > \varepsilon_B \end{cases} \tag{19}$$

Where ε_{cu} is suggested to be 0.02 based on the experimental results by Liang and Fragomeni [27], and β_c is presented by Hu et al. [32] which is as follows:

$$\beta_c = \begin{cases} 1/0 & \dfrac{D}{t} \le 40 \\ 0/0000339 \left(\dfrac{D}{t} \right)^2 - 0/0102285 \left(\dfrac{D}{t} \right) + 1/3491 & 40 < \dfrac{D}{t} \le 150 \end{cases} \tag{20}$$

2.4. Element type and meshing

For the modeling of CFDST, concrete core and steel wall in the software, Continuum or Solid eight-node hexagonal elements having three degrees of transitional freedom in each node were used, with a linear complete integration method represented by 8DR3C in ABAQUS software [34, 35 and 36]. Each element has three degrees of freedom of movement in the X, Y, and Z axis. This element is suitable for linear, nonlinear, complex, contact and plastic analyzes associated with large deformations. In solid three-dimensional elements, material properties can be applied in several layers of varying amounts in different directions. In this program, all solid elements consider the limited strain effects. The limited strain concept means that the substance has non-elastic behavior. In all cases, solids have the ability to accurately determine the amount of stress. Also, in these elements, the stress-strain components are determined in the main axes directions, except for those defined for local axes elements [37]. In the present study, meshing sensitivity was studied to determine the proper mesh [38, 39, 40, and 41]. The maximum mesh size for columns was 20 mm (Fig. 7).

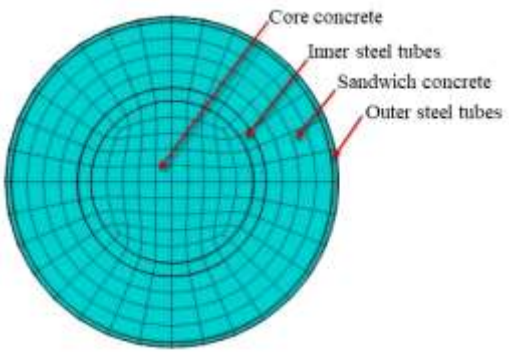

Fig. 7. Illustration of the FE mesh of a CFDST specimen.

2.5. Interaction Model Between Steel and Concrete

The interaction used in the ABAQUS model is surface-to-surface interaction. Each model requires two interactions. The first contact is between the outer tube and the concrete section in which the inner part of the outer tube was the master surface and the outer part of the concrete was the slave surface. Given the hard contact, surface penetration of the concrete to the steel surface in the enclosed areas is minimized and does not allow the tensile stress to pass through the interfacing section [38]. On the other hand, the contact between steel and concrete is considered surface to surface. In this section, Coulomb's frictional model is used [41], which determines the critical shear stress from the equation $\tau_{crit} = \mu P$, in which μ is the coefficient of friction and P is the contact pressure. The coefficient of friction considered between steel and concrete is 0.3 [43].

2.6. Boundary Conditions

In total, two boundary conditions were used for each ABAQUS model. The first condition fixed the RP-Base reference point at the source using the type of displacement/ rotation. The second boundary condition is used for the RP-Load reference point. The column pressure was introduced through the second boundary condition with a value of U3 set to +50 (Fig. 8). It should be noted that the above description loading ensures that the load is evenly distributed over the cross-section above the axially loaded composite column.

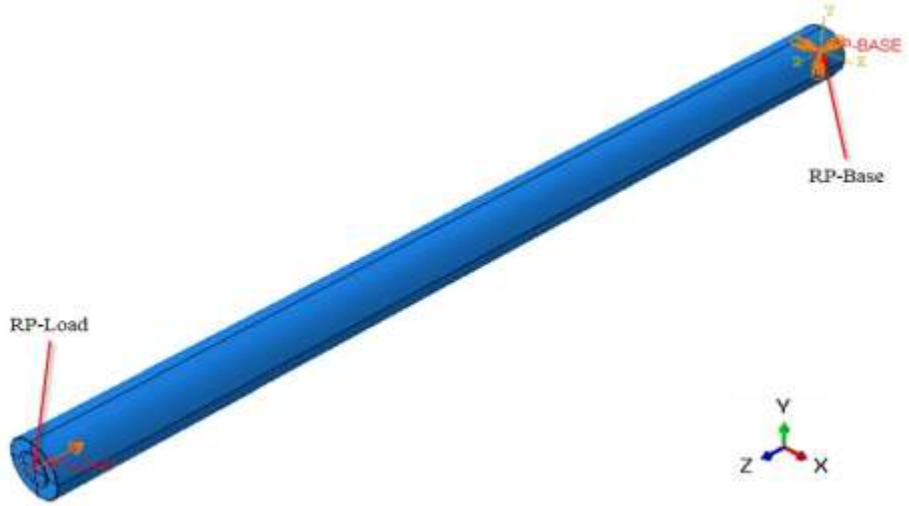

Fig. 8. Load and Boundary Conditions of a typical CFDST specimen.

3. Investigating the Behavior of Double-Skin Composite Columns

3.1. Sample Introduction

In the present study, a total of 20 CFDST columns, with a circular cross-section (CHS-CHS) under axial load, were modeled by ABAQUS software. In this study, the effect of compressive strength of concrete and the effect of increasing the cross section on the inner tube and the effect of increasing the thickness of the internal wall in these columns under axial force have been investigated. Table 3 shows the details of the samples. In Figure 9, the schematic representation of the cross-section of the designed columns is shown. In this table, D_{ext} and t_{ext} are the width and thickness of the outer tube, respectively, D_{int} and t_{int} are the width and thickness of the inner tube, respectively, $f'_{c,ext}$ and $f'_{c,int}$ are the external and internal concrete respectively, and L is the column length. In C220-T3-S30-C110-T6-S80, the first three parameters (C220-T3-S30) specify the outer tube, and the second three parameters (C110-T6-S80) specify the inner tube. The letter C represents a column with a circular cross-section, and the number next to it indicates the dimensions of the column. The letter T represents the thickness of the column, and the letter S indicates the compressive strength of the concrete. Geometric characteristics of the sections are divided into three series according to Table 3. Three series of samples are determined based on the cross-sectional dimension in the inner wall. In Series 1, the cross-section dimensions in the outer tube has a diameter of 220 mm and internal tube has a diameter of 110 mm, and in series 2 and 3, the cross-sectional dimensions are at the outer tube include a diameter of 220 mm and the inner tube is of the size of 132 mm. Also, for each series of samples, the compressive strength of the concrete varies in the inner tube.

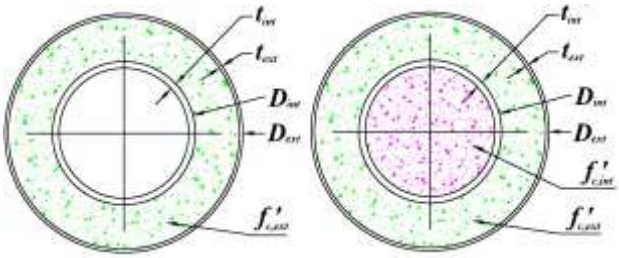

(a) (b)

Fig. 9. Details and dimensions of CFDST specimen; a) Double skin, b) Double tube.

3.2. Effect of Concrete Compressive Strength on Columns

CFDST columns were modeled in finite element software with compressive strength of 0, 30, 40 and 80 MPa in internal wall. Fig. 10 shows the load capacity diagram and Fig. 11 shows the load-displacement diagram. As shown in Fig. 11, increasing the concrete compressive strength increases the axial capacity of the column. In general, the strength and rigidity of CFDST columns increases with increasing concrete strength.

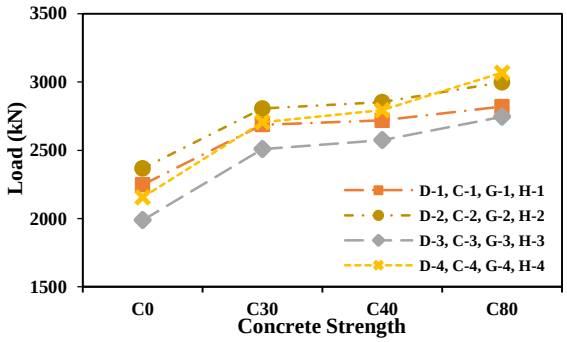

Fig. 10. Load bearing diagram.

The columns with higher strength concrete, in the elastic stage, have more elastic rigidity, as the primary elastic modulus of the concrete increases with the concrete strength.

Table 3. Dimensions of specimens.

ID	Column specimen	Outer tube				Inner tube			
		D_{ext} (mm)	t_{ext} (mm)	$f'_{c,ext}$ (MPa)	L_{ext} (mm)	D_{int} (mm)	t_{int} (mm)	$f'_{c,int}$ (MPa)	L_{ext} (mm)
Series 1									
1-D	C220-T3-S30-S110-T6-S0	220	3	30	3000	110	6	0	3000
1-C	C220-T3-S30-C110-T6-S30	220	3	30	3000	110	6	30	3000
1-G	C220-T3-S30-C110-T6-S40	220	3	30	3000	110	6	40	3000
1-H	C220-T3-S30-C110-T6-S80	220	3	30	3000	110	6	80	3000
2-D	C220-T6-S30-C110-T3-S0	220	6	30	3000	110	3	0	3000
2-C	C220-T6-S30-C110-T3-S30	220	6	30	3000	110	3	30	3000
2-G	C220-T6-S30-C110-T3-S40	220	6	30	3000	110	3	40	3000
2-H	C220-T6-S30-C110-T3-S80	220	6	30	3000	110	3	80	3000
Series 2									
3-D	C220-T3-S30-C132-T6-S0	220	3	30	3000	132	6	0	3000
3-C	C220-T3-S30-C132-T6-S30	220	3	30	3000	132	6	30	3000
3-G	C220-T3-S30-C132-T6-S40	220	3	30	3000	132	6	40	3000
3-H	C220-T3-S30-C132-T6-S80	220	3	30	3000	132	6	80	3000
4-D	C220-T6-S30-C132-T3-S0	220	6	30	3000	132	3	0	3000
4-C	C220-T6-S30-C132-T3-S30	220	6	30	3000	132	3	30	3000
4-G	C220-T6-S30-C132-T3-S40	220	6	30	3000	132	3	40	3000
4-H	C220-T6-S30-C132-T3-S80	220	6	30	3000	132	3	80	3000
Series 3									
3-C-1	C220-3-30-C132-5-80	220	3	30	3000	132	5	80	3000
4-C-1	C220-6-30-C132-2.5-80	220	6	30	3000	132	2.5	80	3000
3-H-1	C220-3-30-C132-5-80	220	3	30	3000	132	5	80	3000
4-H-1	C220-6-30-C132-2.5-80	220	6	30	3000	132	2.5	80	3000

In order to evaluate the change in load capacity of a double-skin column when its internal steel is filled with concrete, according to Table 4, the contribution ratio of the internal concrete (ICCR) provided by Romero et al. [13] is used, which is as follows:

$$ICCR = \frac{N_{u,CFDST,double-tube}}{N_{u,CFDST,double-skin}} \quad (21)$$

According to Fig. 10, by filling the inner tube from concrete, the ductility of the samples is reduced. Also, by increasing the compressive strength of concrete columns up to 80MPa, the ductility of the specimens decreased compared to the columns having 30 and 40 MPa concretes; in other words, due to the brittleness of concrete, ductility of the samples is reduced. This phenomenon may be due to the fact that by increasing the internal skin cross-section, the confinement has also increased. Also, increasing the internal wall cross-section, the total area of the steel utilized in the inner skin also increases which has caused this behavior. This phenomenon may be due to the fact that

by increasing the internal skin cross-section, the confinement has also increased. Also, increasing the internal wall cross-section, the total area of the steel utilized in the inner skin also increases which has caused this behavior.

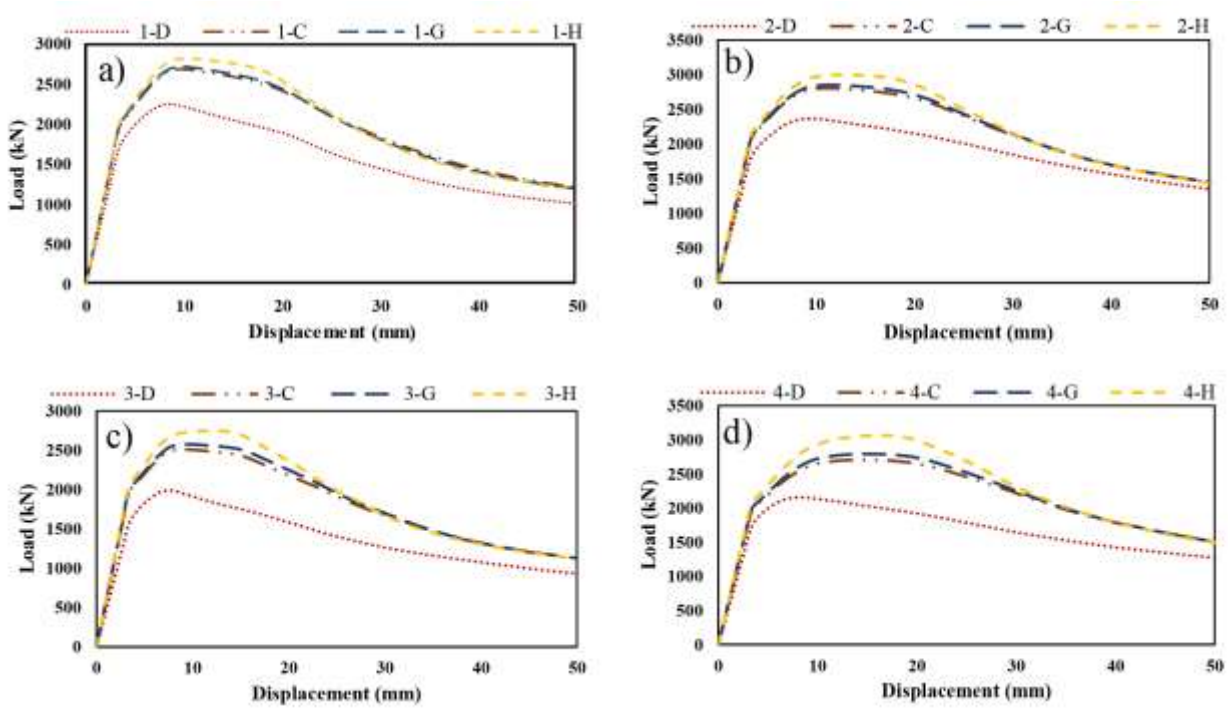

Fig. 11. Load-axial curves for the Compressive strength of concrete.

Table 4. Details of the compressive strength of concrete.

ID	Column specimen	*D/t*	*Δ* (*mm*)	P_{max} (*kN*)	*ICCR*	*(%)	*Energy* (*kJ*)	*Energy Ratio*	**(%)
1-D	C220-T3-S30-C110-T6-S0	66.6	36.17	2247.91	---	---	77.427	---	---
1-C	C220-T3-S30-C110-T6-S30	66.6	28.07	2686.47	1.195	8.89	95.626	1.235	10.51
1-G	C220-T3-S30-C110-T6-S40	66.6	15.88	2718.82	1.209	9.48	95.705	1.236	10.55
1-H	C220-T3-S30-C110-T6-S80	66.6	10.86	2819.19	1.254	11.27	97.295	1.256	11.37
				Avg. =	1.219	9.88	Avg. =	1.242	10.81
2-D	C220-T6-S30-C110-T3-S0	36.3	30.96	2366.56	---	---	91.928	---	---
2-C	C220-T6-S30-C110-T3-S30	36.3	23.80	2804.58	1.185	8.47	106.563	1.159	7.37
2-G	C220-T6-S30-C110-T3-S40	36.3	12.66	2851.73	1.205	9.30	107.626	1.170	7.87
2-H	C220-T6-S30-C110-T3-S80	36.3	6.59	2997.09	1.266	11.75	110.473	1.201	9.16
				Avg. =	1.218	9.84	Avg. =	1.176	8.13
3-D	C220-T3-S30-C132-T6-S0	66.6	25.60	1988.32	---	---	68.345	---	
3-C	C220-T3-S30-C132-T6-S30	66.6	22.28	2509	1.261	11.57	88.878	1.300	13.06
3-G	C220-T3-S30-C132-T6-S40	66.6	13.18	2573.81	1.294	12.83	90.525	1.324	13.96
3-H	C220-T3-S30-C132-T6-S80	66.6	8.97	2745.91	1.381	16.00	93.109	1.362	15.33
				Avg. =	1.312	13.47	Avg. =	1.329	14.11
4-D	C220-T6-S30-C132-T3-S0	36.3	21.13	2156.71	---	---	93.513	---	
4-C	C220-T6-S30-C132-T3-S30	36.3	17.63	2705.45	1.154	11.28	106.799	1.142	6.63
4-G	C220-T6-S30-C132-T3-S40	36.3	10.99	2793.14	1.295	12.85	108.777	1.163	7.545
4-H	C220-T6-S30-C132-T3-S80	36.3	4.67	3066.97	1.422	17.42	114.153	1.221	9.94
				Avg. =	1.290	13.85	Avg. =	1.175	8.03

* Percentage change in bearing capacity

** Percentage change the amount of energy absorbed

3.3. Effect of cross section on the columns

As shown in Fig. 12, studies have shown that in circular sections, with an increase in cross-sectional area by 10%, the bearing capacity is reduced by about 3%. This phenomenon is due to the fact that the cross-section of concrete in the outer wall is lowered and the load is imposed to the sample immediately due to the fact that the inner wall is pressurized on the outside under the axial pressure, which causes the concrete to be crushed, and the enclosure effect of the steel pipes cannot be fully generated. Regarding the diagrams of Fig. 12, it is shown that the enclosure increases the ductility and also maintains the residual resistance until after the columns fail, Table 5 shows the results of the circular samples.

Table 5. Details of the effect of increasing the cross-section on the inner tube.

ID	Column specimen	*D/t*	*Δ* (*mm*)	P_{max} (*kN*)	$\frac{P_{Max}}{P_{Reference}}$	*(%)	*Energy* (*kJ*)	*Energy Ratio*	**(%)
1-C	C220-T3-S30-C110-T6-S30	66.6	28.07	2686.47	---	---	95.705	---	---
3-C-1	C220-T3-S30-C132-T5-30S	66.6	22.76	2343.28	0.872	6.82	84.478	0.882	6.23
1-H	C220-T3-S30-C110-T6-S80	66.6	10.86	2819.19	---	---	97.295	---	---
3-H-1	C220-T3-S30-C132-T5-S80	66.6	9.36	2627.36	0.931	3.52	89.087	0.915	4.40
2-C	C220-T6-S30-C110-T3-S30	36.3	23.80	2804.58	---	---	106.563	---	---
4-C-1	C220-T6-S30-C132-T2.5-S30	36.3	18.17	2681.26	0.956	2.24	106.008	0.994	0.26
2-H	C220-T6-S30-C110-T3-S80	36.3	6.59	2997.09	---	---	110.473	---	---
4-H-1	C220-T6-S30-C132-T2.5-S80	36.3	5.42	3049.48	1.017	0.86	113.493	1.027	1.34
				Avg. =	0.944	3.36	Avg. =	0.954	3.05

* Percentage change in bearing capacity
** Percentage change the amount of energy absorbed

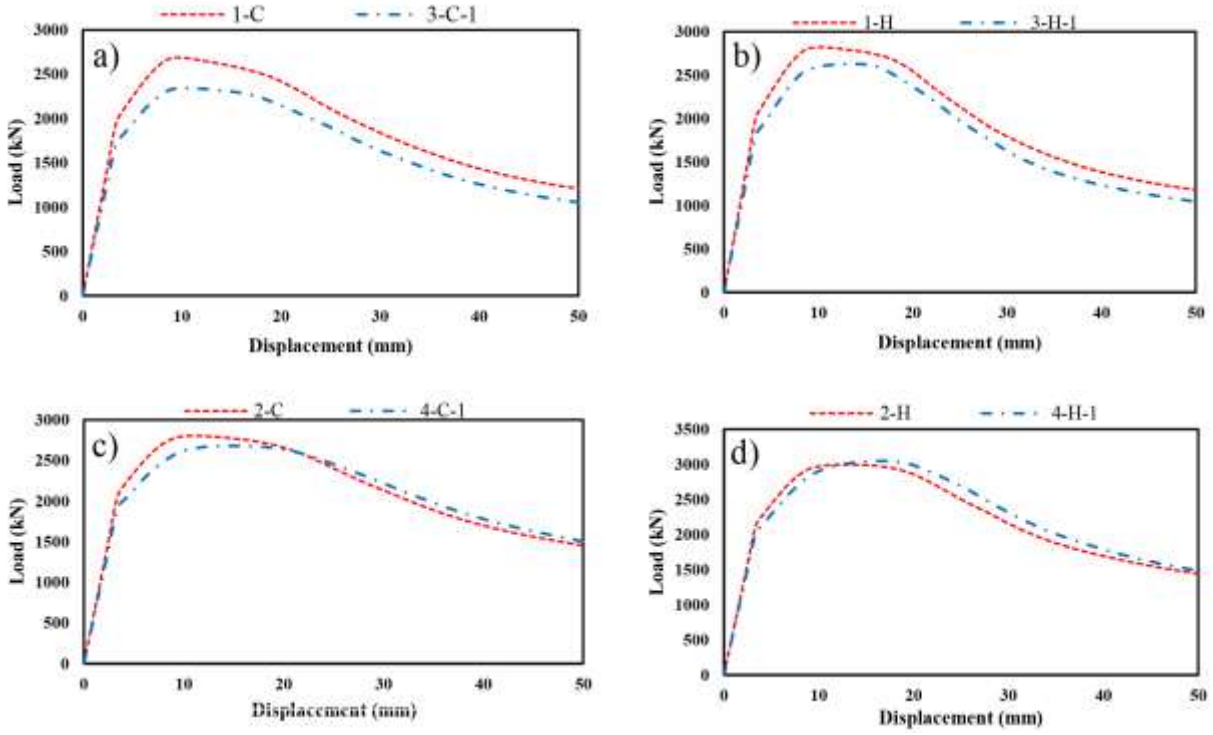

Fig. 12. Load-axial curves for the effect of increasing the cross-section.

3.4. Effect of Thickness on the Inner Wall of the Samples

Figure 13 shows the load–displacement diagram for the columns. As shown in Fig. 13, the thickness of the inner wall decreases with a decrease in the thickness of the columns. Due to the fact that the inner wall contributes in the enclosure of concrete, although less than the outer tube (Fig. 13, parts c and d), by reducing the thickness of the inner tube, samples bear less load capacity, and in columns with less thickness at the outer wall, the bearing capacity is reduced more rapidly according to the plastic region in Fig. 13. Table 6 shows the results of the columns due to the reduction in the thickness of the inner wall.

Table 6. Details of the thickness impact on the inner tube.

ID	Column specimen	*D/t*	Δ (*mm*)	P_{max} (*kN*)	$\frac{P_{Max}}{P_{Reference}}$	*(%)	*Energy* (*kJ*)	*Energy Ratio*	**(%)
3-C	C220-T3-S30-C132-T6-S30	66.6	22.28	2509	---	---	88.878	---	---
3-C-1	C220-T3-S30-C132-T5-S30	66.6	22.76	2343.28	0.933	3.41	84.478	0.950	2.53
3-H	C220-T3-S30-C132-T6-S80	66.6	8.97	2745.91	---	---	93.109	---	---
3-H-1	C220-T3-S30-C132-T5-S80	66.6	9.36	2627.36	0.956	2.21	89.087	0.956	2.21
4-C	C220-T6-S30-C132-T3-S30	36.3	17.63	2705.45	---	---	106.799	---	---
4-C-1	C220-T6-S30-C132-T2.5-S30	36.3	18.17	2681.26	0.991	0.45	106.008	0.992	0.37
4-H	C220-T6-S30-C132-T3-S80	36.3	4.67	3066.97	---	---	114.153	---	---
4-H-1	C220-T6-S30-C132-T2.5-S80	36.3	5.42	3049.48	0.994	0.28	113.493	0.994	0.28
				Avg. =	0.968	1.59	Avg. =	0.973	1.35

* Percentage change in bearing capacity
** Percentage change the amount of energy absorbed

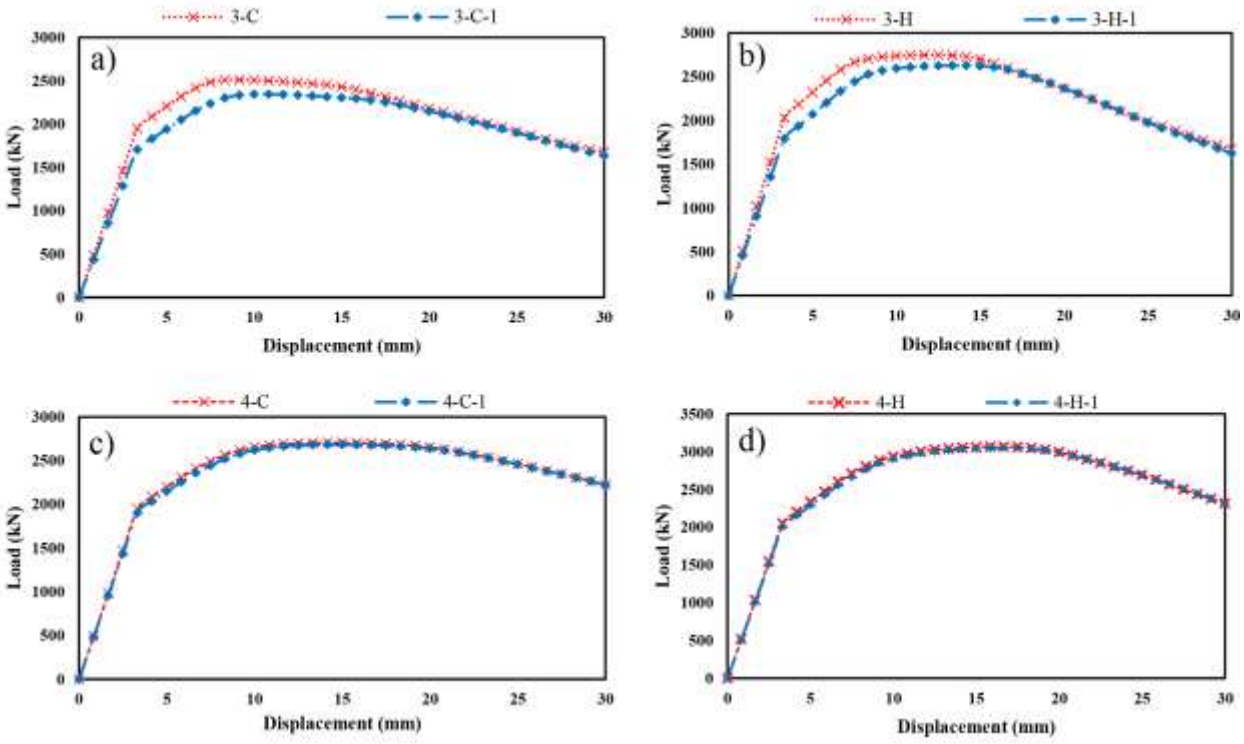

Fig. 13. Load-axial curves for the thickness effect on the inner tube.

4. Models Comparison

As shown in Fig. 14, studies showed that in circular CFDST columns, the effect of thickness changes in steel walls is such that as the thickness of the outer tube increases, the bearing capacity in the specimens increased. Also, by increasing the cross-section of the inner wall by 10%, the bearing capacity decreases by about 3% due to the reduction of the concrete cross-section on the outer tube.

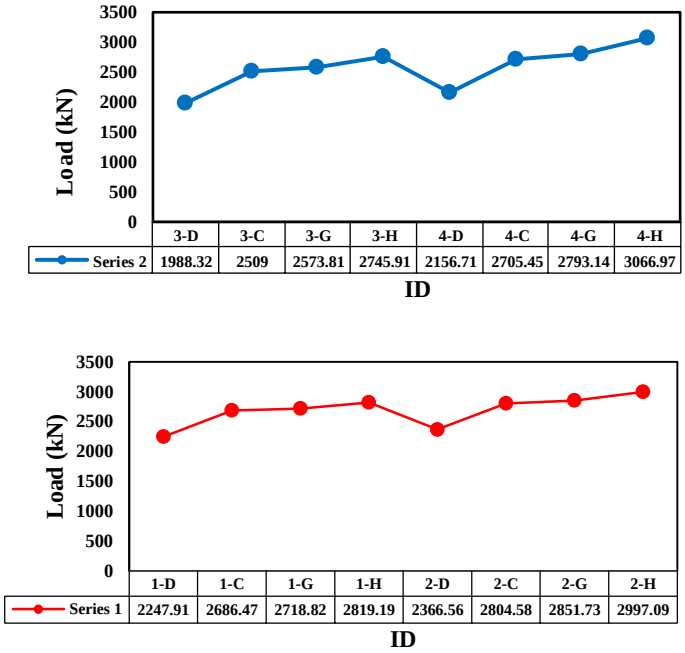

Fig. 14. Load bearing diagram of the samples.

5. Conclusions

In this paper, the effect of compressive strength of concrete on the axial performance of CFDST columns has been investigated. Initially, previous research on the design of CFDST columns was investigated. The ABAQUS 2016 finite element software was used for nonlinear analysis and the accuracy of proposed modeling was compared by the analytical and experimental results. The samples were divided into three series as First Series, Second Series and Third Series. In this paper, a total of 20 samples with circular sections have been investigated by varying the compressive strength of the inner wall, increasing the cross section in the inner wall and also the thickness effect. Circular columns have two different sections, with the first cross-section dimensions of 220 mm in the outer wall and 110 mm of diameter at the inner wall, and the second section, having a diameter of 220 mm at the outer wall and a diameter of 132mm at the inner wall. Also thicknesses of 2.5, 3, 5 and 6 mm are considered for steel in internal and external walls of circular sections. The following general results can be derived from the research presented in this paper:

1- Studies have shown that bearing capacity of CFDST columns increases with increasing compressive strength of concrete in internal wall.

2. Studies showed that in circular sections, with an increase in cross section in the inner wall by 10%, the bearing capacity decreased by about 3%. This phenomenon is due to the

fact that the cross-section of concrete in the outer wall is less and the load is imposed on the sample immediately, since the internal wall is pressurized under axial pressure, which causes the concrete to be crushed.

3- Studies have shown that in CFDST columns, increasing the compressive strength of concrete is not suitable for increasing the load capacity and ductility, due to the brittle properties of concrete in high strengths, which reduces the ductility of the sample. These results indicate that increasing the strength of concrete cannot be a very effective way to improve the performance of CFDST columns.

4- Investigations showed that in circular sections, by reducing the thickness of the inner wall by 10%, the bearing capacity is reduced by about 1.59%.

5- The effect of changes in the steel wall thickness in the CFDST columns is such that the increase in the outer wall thickness is more effective in increasing the bearing capacity of the columns.

6- Studies have shown that concrete confinement is one of the most important features of this type of columns, which ignoring these issues leads to far less than the actual capacity of these columns. The circular steel tube leads the infill concrete to be stressed in triaxial state and as a result confined concrete attains greater compression performance over the performance of the same concrete in unconfined condition.

7- Studies have shown that changes in external thickness are more important because, by increasing the thickness of the outer wall, the bearing capacity of the columns increases, which also increases the enclosure effects.

8- By studying the results, it was found that the circular columns with no concrete core show better ductility than columns with concrete core.

REFERENCES

[1] Zhao, X.L., Han, L.H. (2006). “Double skin composite construction.” Progress in Structural Engineering and Materials, Vol. 8, NO. 3, pp. 93-102. https://doi.org/10.1002/pse.216

[2] Ho, J.C.M. and Dong, C.X. (2014). “Improving strength, stiffness and ductility of CFDST columns by external confinement.” Thin-Walled Structures, Vol. 75, pp.18–290. https://doi.org/10.1016/j.tws.2013.10.009

[3] Subramoni, P.T., Saratha, J.P. (2018). “Behaviour of Beam-Column Subjected to Reversed Lateral Loading, KSCE Journal of Civil Engineering.” Vol. 22, NO. 7, pp. 2464–2468.

https://doi.org/10.1007/s12205-017-2023-6

[4] Zhao, XL., Grzebieta, R. (2002). “Strength and ductility of concrete filled double skin (SHS inner and SHS outer) tubes.” Thin-Walled Struct, 40:199–213. https://doi.org/10.1016/S0263-8231(01)00060-X

[5] Elchalakani, M., Zhao, XL., Grzebieta., R. (2002). “Tests on concrete filled double-skin (CHS outer and SHS inner) composite short columns under axial compression.” Thin-Walled Struct, Vol. 40(5), pp. 415–41. https://doi.org/10.1016/S0263-8231(02)00009-5

[6] Tao, Z., Han, L.H., Zhao, X.L. (2004). “Behavior of concrete-filled double skin (CHS inner and CHS outer) steel tubular stub columns and beam-columns.” Journal of Constructional Steel Research, Vol. 60, NO. 8, pp. 1129-1158. https://doi.org/10.1016/j.jcsr.2003.11.008

[7] Han, L.H., Li, Y.J. Liao, F.Y. (2011). “Concrete-filled double skin steel tubular (CFDST) columns subjected to long-term sustained loading, Thin Walled Structures.” Vol. 49, NO. 12, pp. 1534-1543.

https://doi.org/10.1016/j.tws.2011.08.001

[8] Essopjee, Y. and Dundu, M. (2015). "Performance of concrete-filled double-skin circular tubes in compression." Composite Structures, Vol. 133, pp. 1276–83. https://doi.org/10.1016/j.compstruct.2015.08.033

[9] Romero, M.L., Espinos, A., Portolés, J.M., Hospitaler, A. Ibañez, C. (2015). "Slender double-tube ultra-high strength concrete-filled tubular columns under ambient temperature and fir." Engineering Structures, Vol. 99, pp.536–45. https://doi.org/10.1016/j.engstruct.2015.05.026

[10] Ibañez, C., Romero, M.L., Espinos, A., Portolés, J.M. Albero, V. (2017). "Ultra-high strength concrete on eccentrically loaded slender circular concrete-filled dual steel columns." Structures, Vol. 12, pp. 64-74. https://doi.org/10.1016/j.istruc.2017.07.005

[11] Wan, C.G., Zha, X.X., Dassekpo, J.B.M. (2017). "Analysis of axially loaded concrete filled circular hollow double steel tubular columns exposed to fire." Fire Safety Journal, Vol. 88, pp. 1–12. https://doi.org/10.1016/j.firesaf.2016.12.007

[12] Ekmekyapar, T., Ghanim Hasan, H. (2019). "The influence of the inner steel tube on the compression behaviour of the concrete filled double skin steel tube (CFDST) columns." Marine Structures, Vol. 66, pp. 197–212. https://doi.org/10.1016/j.marstruc.2019.04.006

[13] Lia, W., Cai, Y-X. (2019). "Performance of CFDST stub columns using high-strength steel subjected to axial compression." Thin-Walled Structures, Vol. 141, pp. 411–422. https://doi.org/10.1016/j.tws.2019.04.021

[14] Vernardos S., Gantes Charis. (2019). "Experimental behavior of concrete-filled double-skin steel tubular (CFDST) stub members under axial compression: A comparative review." Structures, Vol. 22, pp. 383–404. https://doi.org/10.1016/j.istruc.2019.06.025

[15] Elchalakani, M., Patel, V.I., Karrech A., Hassanein M.F., Fawzia S., Yang., B. (2019). "Finite element simulation of circular short CFDST columns under axial compression." Structures, Vol. 20, pp. 607–619. https://doi.org/10.1016/j.istruc.2019.06.004

[16] Romero, M.L., Ibañez, C., Espinos, A., Portolés, J.M. and Hospitaler, A. (2017). "Influence of Ultra-High Strength Concrete on Circular Concrete-filled Dual Steel Columns." Structures, Vol. 9, pp. 13-20. https://doi.org/10.1016/j.istruc.2016.07.001

[17] Elchalakani, M., Patel, V.I., Karrech, A., Hassanein, M.F., Fawzia, S., Yang, B. (2019). "Finite element simulation of circular short CFDST columns under axial compression." Structures, Vol. 20, pp. 607-619. https://doi.org/10.1016/j.istruc.2019.06.004

[18] AISC: American Institute of Steel Construction. (2010). Specification for Structural Steel Buildings, ANSI/AISC 360-10.

[19] Aslani, F., Uy, B., Tao, Z., Mashiri., F. (2015). "Behaviour and design of composite columns incorporating compact high-strength steel plates." Journal of Constructional Steel Research, 107, 94–110. https://doi.org/10.1016/j.jcsr.2015.01.005

[20] ABAQUS Standard. User's manual the Abaqus software is a product of dassault systèmes simulia corp. Providence, RI: USA Dassault Systèmes; 2014. Version 6.14, USA.

[21] Xiong, M-X., Xiong, D-X. and Richard Liew, J.Y. (2017). "Axial performance of short concrete filled steel tubes with high and ultra-high-strength materials. Engineering Structures." Vol. 136, pp. 494–510.

https://doi.org/10.1016/j.engstruct.2017.01.037

[22] Bagheri, M., Chahkandi, A. & Jahangir, H. (2019). "Seismic Reliability Analysis of RC Frames Rehabilitated by Glass Fiber-Reinforced Polymers." International Journal of Civil Engineering 17, 1785–1797. https://doi.org/10.1007/s40999-019-00438-x

[23] Wan, C-Y., Zha, X-X. (2016). "Nonlinear analysis and design of concrete-filled dual steel tubular columns under axial loading." Steel and Composite Structures, Vol. 20, No. 3, 571-597. https://doi.org/10.12989/scs.2016.20.3.571

[24] Pagoulatou, M., Sheehan, T., Dai, X.H., Lam, D. (2014). "Finite Element Analysis on the Capacity of Circular Concrete-Filled Double-Skin Steel Tubular (CFDST) Stub Columns." Engineering Structures, Vol. 72, pp. 102-112. https://doi.org/10.1016/j.engstruct.2014.04.039

[25] Naderpour, H., K. Nagai, P. Fakharian, and M. Haji. (2019). "Innovative models for prediction of compressive strength of FRP-confined circular reinforced concrete columns using soft computing methods." Composite Structures, Vol. 215, pp. 69-84. https://doi.org/10.1016/j.compstruct.2019.02

[26] Hassanein, M.F. and Patel, V.I. (2018). "Round-Ended Rectangular Concrete-Filled Steel Tubular Short Columns: FE Investigation Under Axial Compression." Journal of Constructional Steel Research, Vol. 140, pp. 222-236. https://doi.org/10.1016/j.jcsr.2017.10.030

[27] Liang, Q.Q. and Fragomeni, S. (2009). "Nonlinear Analysis of Circular Concrete-Filled Steel Tubular Short Columns under Axial Loading." Journal of Constructional Steel Research, Vol. 65, NO. 12, pp. 2186-2196. https://doi.org/10.1016/j.jcsr.2009.06.015

[28] Mander, J.B., Priestley, M.J.N. and Park, R. (1988). "Theoretical Stress-Strain Model for Confined Concrete." Journal of structural Engineering, ASCE, Vol. 114, NO. 8, pp. 1804-1826. https://doi.org/10.1061/(ASCE)0733-9445(1988)114:8(1804)

[29] American Concrete Institute, (2011). Building Code Requirements for Structural Concrete (ACI 318−11) and Commentary.

[30] Liang, Q.Q. (2009). "Performance-Based Analysis of Concrete-Filled Steel Tubular Beam-Columns, Part I: Theory and Algorithms." Journal of Constructional Steel Research, Vol. 65, pp. 363-372. https://doi.org/10.1016/j.jcsr.2008.03.007

[31] Richart, F.E., Brandtzaeg, A. Brown, RL. (1928). "A study of the failure of concrete under combined compressive stresses, Bull 185, Champaign (III): University of Illionis." Engineering Experimental Station; Vol. 185. http://hdl.handle.net/2142/4277

[32] Hu, H.T., Huang, C.S., Wu, M.H. and Wu, Y.M. (2003). "Nonlinear Analysis of Axially Loaded Concrete-Filled Tube Columns with Confinement Effect." Journal of Structural Engineering, ASCE, Vol. 129, NO. 10, pp. 1322-1329. https://doi.org/10.1061/(ASCE)0733-9445(2003)129:10(1322)

[33] Tang, J., Hino, S., Kuroda, I. and Ohta, T. (1996). "Modeling of stress-strain relationships for steel and concrete in concrete filled circular steel tubular columns." Steel Construction Engineering, JSSC, Vol. 3 NO. 11, pp. 35-46. https://doi.org/10.11273/jssc1994.3.11_35

[34] Yao, Y., Liu, M. Guo, H. (2019). "Concrete filled double skin steel tubular columns subjected to non-uniform heating." Journal of Constructional Steel Research, Vol. 158, pp. 263–278. https://doi.org/10.1016/j.jcsr.2019.03.035

[35] Alhalaby, M. Wanga, Y. (2017). "Second-order effects of cantilever concrete filled double skin tube (CFDST) transmission towers." Copenhagen, Denmark, Vol. 1, pp. 4390-4399. https://doi.org/10.1002/cepa.498

[36] Wang, F-C., Han, L-H. (2019). "Analytical behavior of carbon steel-concrete-stainless steel double skin tube (DST) used in submarine pipeline structure." Marine Structures, Vol. 63, pp. 99–116.

https://doi.org/10.1016/j.marstruc.2018.09.001

[37] Schneider, S.P., Alostaz, Y.M. (1998). "Experimental Behavior of Connections to Concrete-filled Steel Tubes." Journal of Constructional Steel Research, Vol. 45, NO. 3, pp. 321-352. https://doi.org/10.1016/S0143-974X(97)00071-0

[38] Hassanein, M.F., Elchalakani, Karrech, M.A., Patel, V.I. and Yang, B. (2018). "Behaviour of Concrete-filled Double-skin Short Columns Under Compression Through Finite Element Modelling: SHS Outer and SHS Inner Tubes." Structures, Vol. 14, pp. 358-375. https://doi.org/10.1016/j.istruc.2018.04.006

[39] Pons, D., Espinós, A., Albero, V., Romero, M.L. (2018). "Numerical study on axially loaded ultra-high strength concrete-filled dual steel columns." Steel and Composite Structures, Vol. 26, NO. 6, pp. 705-717. https://doi.org/10.12989/scs.2018.26.6.705

[40] Li, W., Han, L-H., Zhao, X-L. (2015). "Behavior of CFDST stub columns under preload, sustained load and chloride corrosion." Journal of Constructional Steel Research, Vol. 107, pp. 12-23. https://doi.org/10.1016/j.jcsr.2014.12.023

[41] Jahangir, H., Esfahani, M.R. (2018). "Numerical Study of Bond – Slip Mechanism in Advanced Externally Bonded Strengthening Composites." KSCE Journal of Civil Engineering 22, 4509–4518. https://doi.org/10.1007/s12205-018-1662-6

[42] Han, L-H., Yao, G-H., Tao, Z. (2007) "Performance of concrete-filled thin-walled steel tubes under pure torsion." Thin-Walled Structures, Vol. 45, pp. 24–36. https://doi.org/10.1016/j.tws.2007.01.008

[43] Johanssont, M. and Gylltoft, K. (2001). Structural behavior of slender circular steel-concrete composite columns under various means of load application. Steel and Composite Structures, Vol. 1, pp. 393-410. https://doi.org/10.12989/scs.2001.1.4.393